RESEARCH ARTICLE
SPACE PHYSICS: MAGNETOSPHERIC PHYSICS

Earth and Planetary Physics
10: 291–301, 2026
doi: 10.26464/epp2026021

Coordinated observations on the spatiotemporal development of global-scale dipolarizations and their coupling to meso-scale dipolarizations

Sheng Tian[1,2*], J. M. Weygand[3], J. Liu[2,3], J. R. Wygant[1], L. Lyons[2], V. Angelopoulos[3], J. Bortnik[2], and G. D. Reeves[4]

[1]School of Physics and Astronomy, University of Minnesota, Minneapolis, Minnesota, USA;

[2]Department of Atmospheric and Oceanic Sciences, University of California, Los Angeles, California, USA;

[3]Institute of Geophysics and Planetary Physics, University of California, Los Angeles, California, USA;

[4]Los Alamos National Laboratory, Los Alamos, New Mexico, USA

Key Points:

- Global-scale dipolarizations are enduring (20–30 min), slow (2–4 deg/min), and global (12 h local time).
- Meso-scale dipolarizations are bursty (several minutes), fast (several tens deg/min), and local (several hours local time).
- Meso-scale dipolarizations tend to occur around the expanding edge of the global-scale dipolarization.

Citation: Tian, S., Weygand, J. M., Liu, J., Wygant, J. R., Lyons, L., Angelopoulos, V., Bortnik, J., and Reeves, G. D. (2026). Coordinated observations on the spatiotemporal development of global-scale dipolarizations and their coupling to meso-scale dipolarizations. *Earth Planet. Phys.*, *10*(2), 291–301. http://doi.org/10.26464/epp2026021

Abstract: Global- and meso-scale dipolarizations are well-known features of Earth's magnetosphere, but their coupling remains poorly understood. Here, using a new approach that combines two-dimentional (2D) ionospheric field-aligned current (FAC) maps with coordinated observations from a network of magnetospheric satellites, we directly show that individual global-scale dipolarizations can expand from the nightside to, or even into, the dayside. These expansions are enduring (20–30 minutes), slow (2–4 deg/min), and global in extent (up to 12 h in local time), consistent with previous statistical inferences but now explicitly observed. The expanding FACs form a two-sheet current system as described by the Boström II model. In contrast, meso-scale dipolarizations are bursty (a few minutes), fast (several tens deg/min), and localized (several hours in local time), as evidenced by auroral expansions and satellite data. They are associated with the line-current system as described by the Boström I model (i.e., the substorm current wedge). Notably, meso-scale dipolarizations often emerge near the expanding edge of a global-scale dipolarization, suggesting a dynamic coupling between the two scales. These observations provide a complementary scenario to the simulation-based interpretation that global-scale dipolarizations result from the accumulation of meso-scale dipolarizations. Here, meso-scale dipolarizations appear far less frequently than in simulations and occur around the edge of global-scale dipolarizations. This result implies that meso-scale dipolarizations may be sporadically triggered during the azimuthal expansion of global-scale dipolarizations.

Keywords: dipolarization; field-aligned current; magnetosphere–ionosphere coupling

Plain Language Summary

Dipolarization is an energy release process in a magnetized plasma when the magnetic energy is released. Both global-scale dipolarizations and meso-scale dipolarizations occur in the Earth's magnetosphere. Using a new approach that combines observations of the two-dimentional (2-D) ionospheric current and a network of magnetospheric satellites, we can observe the spatiotemporal development of individual global-scale dipolarizations for the first time. They expand azimuthally slowly and divergently and can last 20–30 min, allowing them to reach the dayside. In contrast, meso-scale dipolarizations last for only several minutes and are much more localized. Notably, meso-scale dipolarizations tend to emerge near the expanding edge of a global-scale dipolarization. This result implies that meso-scale dipolarizations may be triggered sporadically during the azimuthal expansion of global-scale dipolarizations.

Correspondence to: S. Tian, ts0110@atmos.ucla.edu
Received 06 AUG 2025; Accepted 27 NOV 2025.
First Published online 12 DEC 2025.

1. Introduction

The solar wind drives global convection of Earth's surrounding plasma and stretches the Earth's dipole field in the nightside (Dungey, 1961). In this picture, magnetic energy is stored and released in geospace in cycles that are coordinated with a global plasma convection, which flows divergently around midnight and azimuthally toward noon. As observations and simulations of the near-Earth space environment improve, the current picture has further included transient earthward flows at several hundreds km/s called the bursty bulk flows (BBFs; Baumjohann et al., 1990;

Angelopoulos et al., 1992), into the global convection. BBFs are important meso-scale structures that are closely related to geomagnetic substorms, when magnetic energy is released in geospace. The cross-scale interaction among substorm phenomena has been a primary focus of the community (e.g., Gabrielse et al., 2019; Merkin et al., 2019; Nishimura et al., 2022, and references therein).

One major substorm feature is the configuration change of magnetic fields in the tail region from stretched to more dipole-like, i.e., dipolarization (Cummings et al., 1968). Two types of dipolarization phenomena, global- and meso-scale dipolarizations, are well known and have been extensively studied. Statistical observations within geosynchronous orbit (6.6 Earth radii, R_E) show that global-scale dipolarizations propagate azimuthally away from local midnight (Nagai, 1982; Ohtani et al., 2018). Beyond 6.6 R_E, nightside observations show that meso-scale dipolarizations propagate earthward with BBFs (Runov et al., 2009, 2011; Liu J et al., 2013, 2014). The meso-scale dipolarization is also commonly referred to as the dipolarization front or the dipolarizing flux bundle (DFB). It is closely related to common substorm phenomena, including particle injection (Gabrielse et al., 2017), and the substorm current wedge (SCW; McPherron et al., 1973; Liu J et al., 2015).

Besides the propagation direction, the global- and meso-scale dipolarizations are different in many aspects. From a single spacecraft measurement, global-scale dipolarizations are characterized by a steady (several tens of minutes) increase in the tilt angle of the magnetic field and remain dipolarized for the next 20–30 min (Nagai, 1982; Ohtani et al., 2018), whereas the meso-scale dipolarizations are typically transient peaks (up to several minutes) in either B_z or the tilt angle. The propagation speed of DFBs is on the order of 500 km/s, mostly Earthward (Liu J et al., 2014). The global-scale dipolarizations propagate at a much slower speed (30–50 km/s around 6.6 R_E, or 2–4 deg/min) and are mostly azimuthal (Nagai, 1982; Ohtani et al., 2018).

Dipolarizations are typically associated with current systems that couple the ionosphere and magnetosphere. Considering whether the ionospheric currents are Pedersen or Hall currents, Boström (1964) proposed two fundamental models of the current system, where the Boström I model consists of line currents driven by a toroidal electric field and the Boström II model consists of sheet currents driven by a poloidal electric field. The meso-scale dipolarization is associated with a wedgelet current (Liu J et al., 2015) that usually develops into a larger-scale SCW (McPherron et al., 1973; Clauer and McPherron, 1974). Both are consistent with the Boström I model. Additional current structures exist around the DFB head that are important in understanding the coupling of meso-scale dipolarizations to the ionosphere (Yao ZH et al., 2013). The global-scale current system is less well understood. There are cases when the global-scale currents follow the Boström II model and when they consist of multiple wedgelets (Nishimura et al., 2020).

Whether and how global- and meso-scale dipolarizations are coupled is not well understood. In addition, the spatiotemporal evolution of individual global-scale dipolarization has not been well studied because the geospace is sparsely probed. Here, with a new approach to study time periods when a network of magnetospheric satellites is in magnetic conjugacy over North America, which is abundantly sampled by ground magnetometers, we can unveil the propagation of individual global-scale dipolarizations. This new approach can explicitly determine the lifetime, propagation speed, and spatial extent of individual global-scale dipolarizations and discuss their potential coupling to meso-scale dipolarizations and processes.

2. Observations

A dipolarization is defined as a sudden increase in the tilt angle of the magnetic field (Cummings et al., 1968). In this study, we formulate this definition into the algorithm described in Supplementary Materials A.

The magnetic field data used in this study are from the magnetometers onboard the following spacecraft in equatorial orbits: the Van Allen Probes (Radiation Belt Storm Probes [RBSP], RBA/B; Kletzing et al., 2013), THEMIS (Time History of Events and Macroscale Interactions during Substorms, THA/B/C/D/E; Auster et al., 2008), GOES (Geostationary Operational Environmental Satellites, G13/14/15; Singer et al., 1996), and MMS (Magnetospheric Multiscale Mission; Torbert et al., 2016). The original data resolution is 8 samples/sec for RBSP, 3 samples/s for THEMIS, 2 samples/s for GOES, and 16 samples/s for MMS. All magnetic field data are downsampled to 10 samples/s to be uniformly processed in this study. In addition to satellite data, we utilize auroral observations from ground-based all-sky imagers (ASIs) (Mende et al., 2008) and FACs as approximated from the spherical elementary current system (SECS) (Amm and Viljanen, 1999; Weygand et al., 2011; Vanhamäki and Juusola, 2020). ASIs provide high-resolution (3-s) images at high spatial resolution (1–5 km) that can resolve small-scale auroral structures. The SECS data are at the cadence of 10 s and the spatial resolution of approximately100–200 km at auroral latitudes. The spatial resolution is adequate to study the global-scale dipolarizations.

2.1 The Propagation of Global-Scale Dipolarizations is Azimuthal

Figure 1 shows a dipolarization event on August 28, 2014. Figures 1a and 1d show that six local dipolarizations were observed by different satellites in an azimuthal ordering, instead of the radial distances. Figure 1c shows an example of how the propagation direction was calculated within the triangle among THD-THE-G15. As explained in Supplementary Materials A, determining the 2D propagation requires at least three satellites in a non-linear configuration (e.g., THD, THE, and THA are linear and cannot be used). The result is an azimuthal propagation speed of 30 km/s. This speed is consistently determined using other available triangles (e.g., RBB-G15-THA) that are not shown.

Figure 1d visualizes the change in the detrended tilt angle θ along the satellite tracks in the time-magnetic local time (MLT) plane. It shows a clear transition from negative to positive θ. The transition follows a uniform global-scale angular speed of 2.1 deg/min. For the relevant radial distances (5–12 R_E), this is consistent with the local speed of 30 km/s from the three-satellite timing. The azimuthal propagation speed is consistent with previous statistical

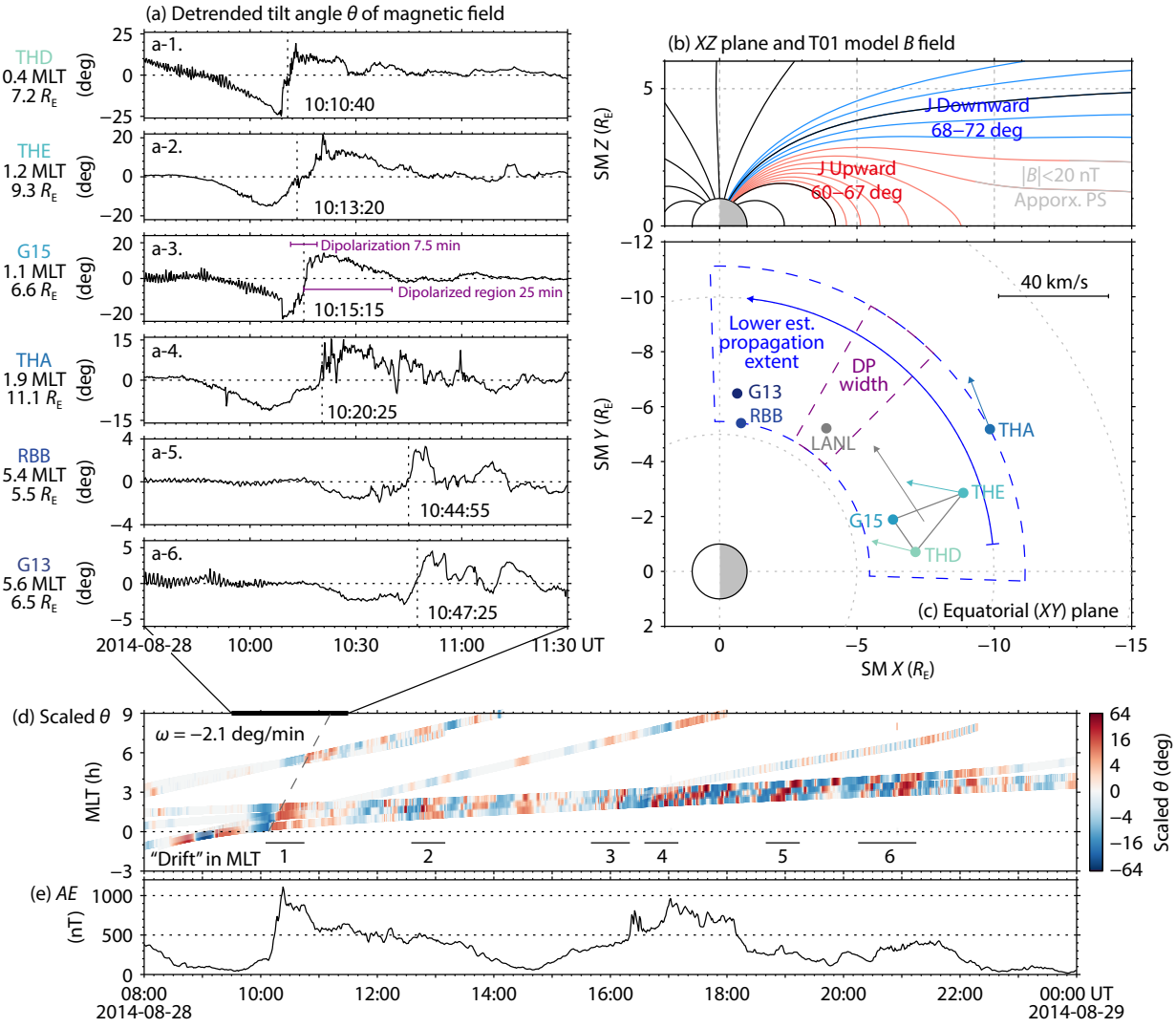

Figure 1. Dipolarizations observed in the order of magnetic local time (MLT) on August 28, 2014. Panel (a) shows the dipolarizations, as characterized by the increasing ramps in θ (the detrended tilt angle of the magnetic field), observed at six spacecraft. Panel (b) shows the magnetic field configuration from the ionosphere to the equatorial magnetosphere. Some field lines are color-coded to indicate the regions of field-aligned currents (FACs). Panel (c) shows the spacecraft locations, the lower estimation of the spatial extent covered by the dipolarizations (dashed blue region), and mean ion velocities (more than 30 min, colored-arrows) in the equatorial plane. The propagation vector (gray) within a local triangle (gray) and the width of the dipolarization (DP, dashed purple region) are also plotted. Panel (d) plots θ, scaled empirically by $e^{(MLT/4)^2/2}$ to compensate for the decay of θ in MLT, along spacecraft tracks in real time and MLT. The six dipolarizations are recognized as a decaying drift in MLT at 2.1 deg/min. Similar "drifts" in MLT at a similar angular speed were repetitively seen at later times. Panel (e) shows the auroral electrojet (*AE*) index, where the sharp increase around 10:10 universal time (UT) indicates the start of a substorm.

studies (Nagai, 1982; Ohtani et al., 2018), but here it is more rigorously determined, including both direction and magnitude, by using the three-satellite timing. In addition, our observation shows that the individual dipolarization can propagate from around midnight to close to the dayside and can last for 27 min. The propagation extent and duration are not shown in previous statistical studies. The change in θ decreased as the MLT drifted away from midnight (Figure 1a). This result is consistent with a decay of strength during the azimuthal propagation of the individual global-scale dipolarization.

Using the observed angular speed, we can, in principle, estimate the azimuthal scale (in angle) of the global-scale dipolarization. However, the shape of the dipolarization clearly decayed and evolved over time (Figure 1a). Here, we use the middle satellite, G15, to estimate the scales very roughly. The duration of the dipolarization (7.5 min, when $d\theta/dt > 0$) converts to 15 deg (Figure 1a-3). Note that the global-scale dipolarization we refer to here is essentially the edge of a dipolarized region that is expanding azimuthally. The azimuthal propagation of the global-scale dipolarization is equivalent to the azimuthal expansion of the dipolarized region (c.f. Figure 4). They will be used interchangeably in this work.

2.2 The Coupling Between Global-Scale Dipolarization and Ionospheric Currents

Figure 2 compares the azimuthal development of the global-scale

dipolarization in the magnetosphere (Figure 2b) and the ionospheric currents (Figures 2d–2e). These examples are chosen during geomagnetic storms, but it is clear that each global-scale dipolarization was closely related to an individual substorm, as characterized by the increase in the *AE* (Auroral Electrojet) index (Figures 2a). The azimuthal propagation of the global-scale dipolarization has an angular speed that is consistent with the azimuthal expansion of the upward and downward FACs.

Figure 2f shows the 2D images of the inferred ionospheric currents, showing the azimuthal expansion of a two-sheet current system of FACs, with the upward current at a higher latitude than the downward current (Figure 2c). The two-sheet current system is the Boström II model (Boström, 1964). The Boström I model is a two-line current system that is physically different. The SWC is an example of the Boström I model.

The observations in Figure 2 show that a global-scale dipolarization is coupled to the ionosphere through two-sheet FACs. This is a coupled system that expands or propagates azimuthally at all altitudes. Specifically, Figure 2f shows snapshots of the ionospheric currents before (f-1), during (f-2 and f-3), and after (f-4) the azimuthal propagation. The times of the snapshots are marked in Figure 2e-3 (short vertical bar below the panel). The original FAC pattern, which is consistent with the classical Region 1 and Region 2 currents (Iijima and Potemra, 1978; Figure 2f-1), developed into the two-sheet FACs, which enhanced in strength, expanded in local time (Figures 2f-2 and 2f-3), and later recovered (Figure 2f-4).

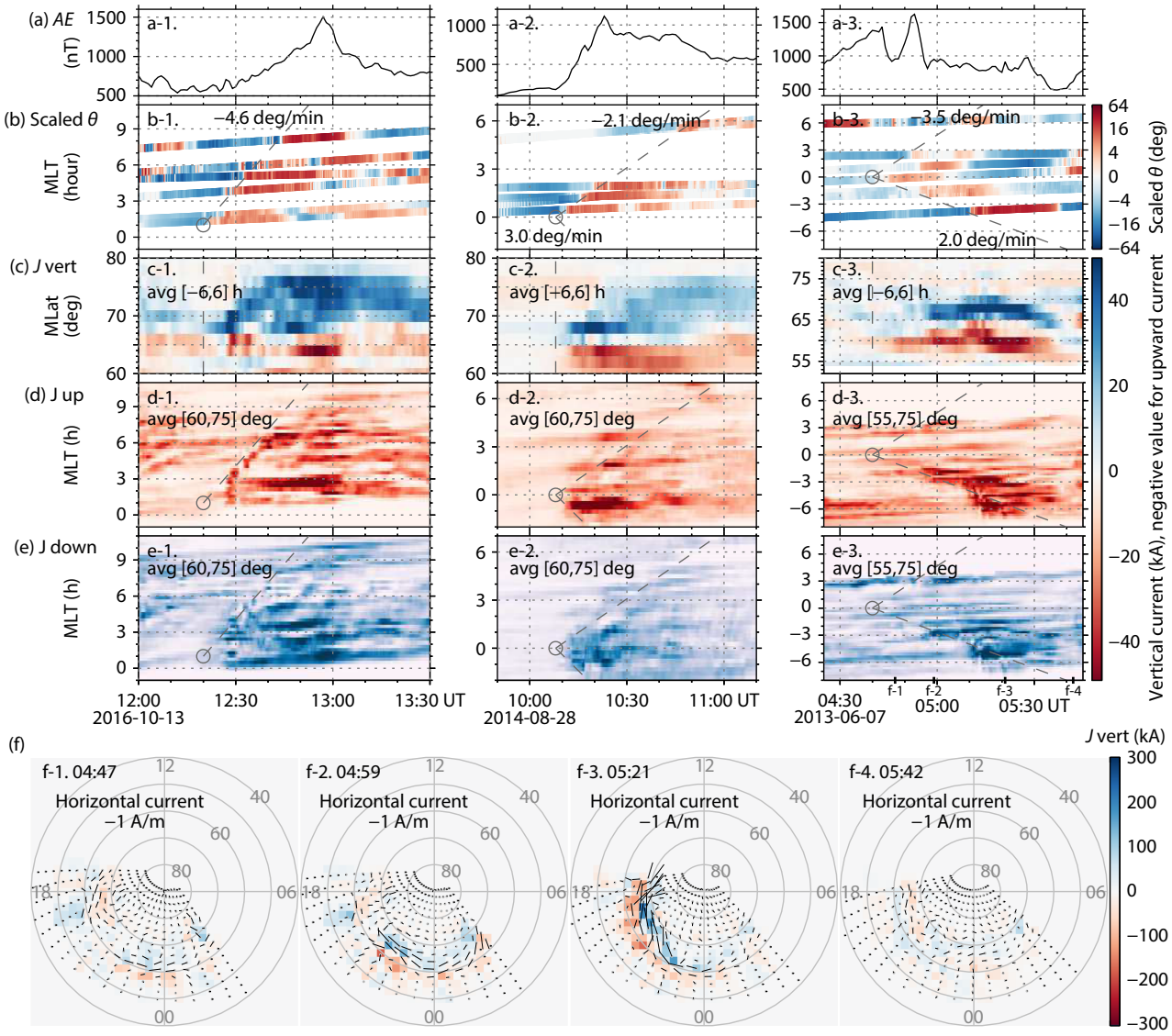

Figure 2. The divergent and azimuthal propagation of dipolarizations and FACs. Panel (a) shows the *AE* index. Panel (b) shows the scaled θ in the same format as in Figure 1. Panels (c) to (e) shows the temporal evolution of FACs in magnetic latitude (MLat) and MLT. In Panels (b), (d), and (e), the same circles and dashed lines are used to mark the origin and angular speed of the global-scale dipolarizations. Panel (f) shows the 2D currents at the four marked times. Arrows denote the horizontal currents (dots mark the origin of the vectors, not the head). J up and J down in Panels (d) and (e) are the upward and downward FACs, respectively. *J* vert in Panels (c) and (f) is the vertical current that is horizontal to the ground.

Note that the snapshots are deliberately chosen to show the pre-midnight sector, where the classical Region 1 and Region 2 currents are in opposite directions to the observed two-sheet FACs. Associated with the two-sheet FACs, a westward horizontal current, called the auroral electrojet, was seen to enhance and expand accordingly (Figures 2f-2 and 2f-3).

2.3 The Coupling Between Global- and Meso-scale Dipolarizations

The August 28, 2014 event shown in Figure 1 contains two distinct impulsive energy releases around 10:10 UT and 10:20 UT, which are shown in more detail in Figure 3. In the first energy release, THD and THE observed Poynting flux bursts flowing along the magnetic fields toward the ionosphere (black, Figures 3a-1 and 3a-2) and BBFs flowing across the magnetic fields toward the Earth (red, same panels). In addition, G15 observed a dispersionless change in the flux of keV electrons (Figure 3a-4). This could be a dispersionless injection or a signature of dipolarization. Ground-based all-sky imagers captured an auroral expansion starting around 0 h MLT and expanding to ±1 h MLT (Figure 3b). The auroral expansion is presumably associated with the first BBF around 10:10 UT and is powered by the associated Poynting flux.

In the second energy release, a BBF, Poynting flux (Figures 3a-1 to 3a-3), and dispersionless change of keV electron flux (LANL [Los Alamos National Laboratory] 191-080; Figure 3a-5) were also observed. To date, it has been well known that all these features are inter-correlated. Specifically, a meso-scale dipolarization is the Earthward front of the BBF (Liu J et al., 2013, 2014). The BBF is coupled to the ionosphere through SCW-like FACs (Liu J et al., 2015). The BBF travels from the magnetotail to the near-Earth region and is related to the onset of the auroral expansion (Nishimura et al., 2011) and injections (Gabrielse et al., 2017; Ukhorskiy et al., 2018). The auroral intensification and motion are driven by the Alfvénic Poynting flux bursts (Wygant et al., 2000; Keiling et al., 2003; Tian S et al., 2021).

The meso-scale dipolarization, and the associated features, including the BBF, SCW, Poynting flux bursts, and possibly injection, are all meso-scale and transient. The two BBFs are meso-scale because the first one was seen only by THD and THE (Figures 3a-1 and 3a-2), and the second one was seen only by THE and THA (Figures 3a-2 and 3a-3). From the location of these satellites (Figure 1d), both BBFs are at most 2 R_E wide. The first one was around 0–2 h MLT, and the second one was around 2–4 h MLT. The auroral expansion, as seen from the snapshots in Figures 3b-1 to 3b-3, was up to 2 h in local time. Therefore, the associated SCW and Poynting flux are likely to be localized (McPherron et al., 1973; Clauer and McPherron, 1974; Tian et al., 2021). The expansion was approximately 20 deg/min (Figure 3b-4), but lasted only for 4 min. This duration is transient as compared with the duration of 20–30 min of a global-scale dipolarization. Similarly, the durations of the BBF and Poynting flux were also several minutes (Figures 3a-1 to 3a-3).

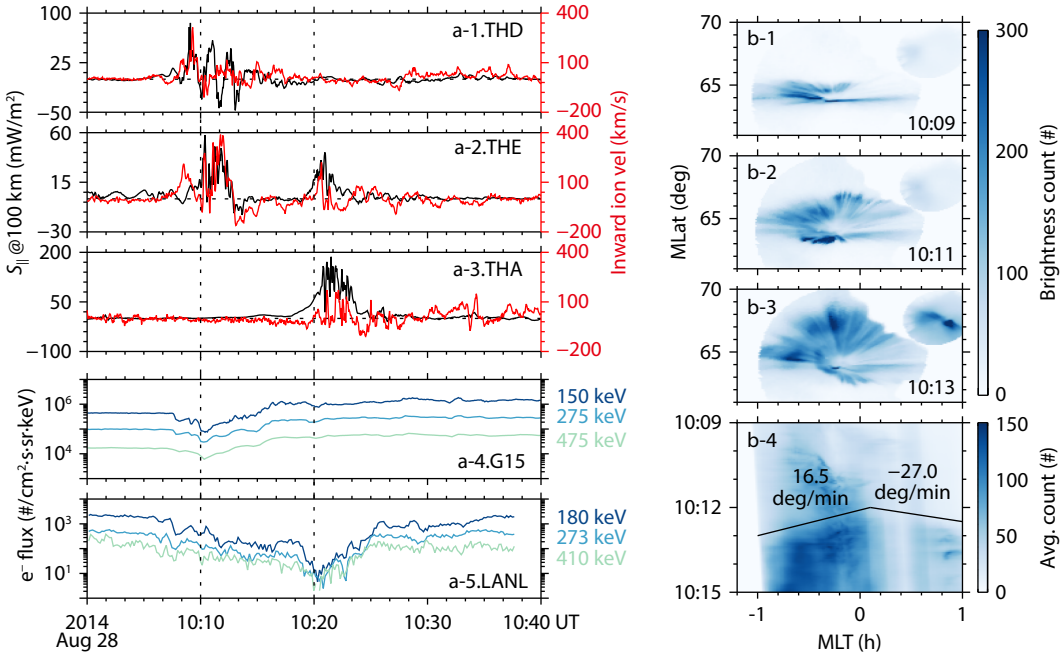

Figure 3. Two meso-scale energy-releasing processes occurred around 10:10 UT and 10:20 UT in the August 28, 2014, event, each involving wave Poynting flux, BBF, injection of keV electrons into the magnetosphere, and auroral expansion in the ionosphere. Panels (a-1) to (a-3) show the THD, THE, and THA measurements on the parallel Poynting flux (normalized to 100 km altitude to account for the focusing along the magnetic field lines) and the ion velocity along the radially inward direction. $S_{||}$ is the Poynting flux parallel to the background magnetic field. Panels (a-4) and (a-5) show the fluxes of keV electrons measured by the G15 and LANL 1991-080 spacecraft. Panels (b-1) to (b-3) show snapshots of the 2D auroral images at 10:09, 10:11, and 10:13 UT. Panel (b-4) shows the ewogram of the 2D auroral images to quantify the eastward and westward motions. At each MLT bin, the value is averaged over [61,70] deg in MLat. The lines in Panel (b-4) are eye guides and are shifted upward to avoid overlapping the expanding aurora.

In summary, we observed two localized BBFs during the azimuthal expansion of a global-scale dipolarization. Each BBF was associated with a high-speed (several hundreds km/s) flow. The BBF and its DFB (the front of the BBF) are thus propagating primarily Earthward. Besides the Earthward propagation, there was a fast (20 deg/min) azimuthal expansion of the meso-scale dipolarization, characterized by the auroral expansion, which was likely to have been triggered by the BBF. A similar association between the fast azimuthal propagation of dipolarizations and auroral expansion has been well-documented (Angelopoulos et al., 2008; Ogasawara et al., 2011).

The meso-scale and global-scale dipolarizations, as observed in the August 28, 2014, event, are very different in duration, expansion speed, and spatial extent. However, they are probably coupled features because the second meso-scale dipolarization (around 2–4 h MLT) was eastward of the first one (around 0–2 h MLT). Both meso-scale dipolarizations were around the expanding edge of the global-scale dipolarization. A similar coincidence was observed in the June 07, 2013, event and was published by Tian S et al. (2021). In this event, a global-scale dipolarization expanded westward at 2.0 deg/min (Figure 2b-3) and a meso-scale dipolarization expanded westward at 13.6 deg/min, as characterized by the auroral expansion and Poynting flux (Tian S et al., 2021).

3. Discussion

3.1 The Propagation of Global-Scale Dipolarizations is Azimuthal

Magnetic flux pileup (Baumjohann et al., 1999; Nakamura et al., 2011), which is a feature proposed to occur that is related to dipolarization, is not observed in this event based on the following evidence. First, the three-satellite timing shows that the propagation is mostly azimuthal. No significant tailward propagation occurs. Second, the azimuthal propagation is consistent with the azimuthal convection as indicated by the THEMIS ion velocity measurement. The colored arrows in Figure 1c mark the averaged ion velocities, which are either mostly azimuthal (THA) or have a finite Earthward component (THD and THE). The long term average is more than 30 min, to minimize transient flows and thus to extract the mean global convection (Wang C-P et al., 2006; Kissinger et al., 2012). The Earthward component is due to the Earthward BBFs, as discussed later in the article. The mean ion velocity is comparable to the propagation speed of the global-scale dipolarization, suggesting that the latter is likely to follow the global convection. Given that the dipolarized magnetic fluxes may be convected away from midnight, it is perceivable that no significant magnetic pileup occurs.

Alternatively, the azimuthal timing could be due to multiple earthward DFBs/BBFs occurring in an azimuthal order. In other words, the global-scale dipolarization results from the accumulation of meso-scale dipolarizations (Merkin et al., 2019). However, this scenario is inconsistent with our observations. Figure 3a-2 shows that THE observed two BBFs around 10:10 UT and 10:20 UT, each lasting about 3 min in the spacecraft frame. The two BBFs caused short fluctuations in θ (Figure 1a-2). However, they seem to be only on top of the long and major increase of θ (i.e., the global-scale dipolarization). In addition, over the 30 minutes of the azimuthal propagation of the global-scale dipolarization, only two BBFs were observed around midnight (Figure 3a-1 to 3a-3). Note that THA was beyond 10 R_E during the event. Considering that some BBFs may not reach THA, compared with those that can reach within 8 R_E from the simulation by Merkin et al. (2019), far fewer meso-scale dipolarizations are observed than in the simulation.

Another interesting feature in Figure 1d is the azimuthal "drift" of dipolarizations in general. In the panel, the event we showed is marked by 1, and several groups of dipolarizations (boundary from blue to red, or negative to positive θ) are marked from 2 to 6. These dipolarizations are followed by a much thinner dipolarized region (red, or positive θ). They are likely to be meso-scale dipolarizations that not only propagate Earthward at the speed of several hundreds km/s, but also drift azimuthally following the global convection. Indeed, the azimuthal drift is evidenced from both simulation (Eshetu et al., 2019; Figure A3) and observation of auroral streamers (Tian S et al., 2023).

3.2 The Coupling Between Global-Scale Dipolarization and Ionospheric Currents

The auroral electrojet can either be a Pedersen (Boström I) or Hall (Boström II) current, depending on whether the observed FACs are line or sheet currents, respectively (Boström, 1964). The observation of the two-sheet FACs demonstrates that the global-scale auroral electrojet is a Hall current. This observation seems to contradict the popular model of the SCW, which involves line currents (Boström I; McPherron et al., 1973; Kepko et al., 2015). However, as discussed later in this article, Boström I currents operate in a local (within several hours in MLT) and transient (several minutes) fashion and thus are on a different temporal and spatial scale compared with the global two-sheet FACs associated with the global-scale dipolarization. Similar to how BBFs provide a localized complement to the global convection, the Boström I model provides a localized Pedersen auroral electrojet complement to the global Hall auroral electrojet.

Our tracing of the two-sheet FACs to the magnetospheric equator (Figure 1b) by using the T01 model (Tsyganenko, 2002) shows that the global-scale dipolarization (Figure 1c) mapped directly to the upward FAC and thus also the auroral oval (Fujii et al., 1994). According to the Boström II model, the upward and downward FACs are closed within a vertical plane at a certain MLT, by a Pedersen current in the ionosphere, and by another Pedersen current in the distant magnetotail (Boström, 1964). This result is consistent with the observations that the global-scale dipolarization, FACs, and westward auroral electrojet all developed azimuthally in pace (Figure 2). As summarized in Figure 4, the azimuthal propagation of a vertical plane leads to the azimuthal expansion of the two-sheet FACs (and auroral electrojet) in the ionosphere and the dipolarized region in the magnetosphere. The expanding edge of the dipolarized region is the global-scale dipolarization. The expansion is likely to be both eastward and westward.

3.3 The Coupling Between Global- and Meso-scale Dipolarizations

Whether the global- and meso-scale dipolarizations are physically

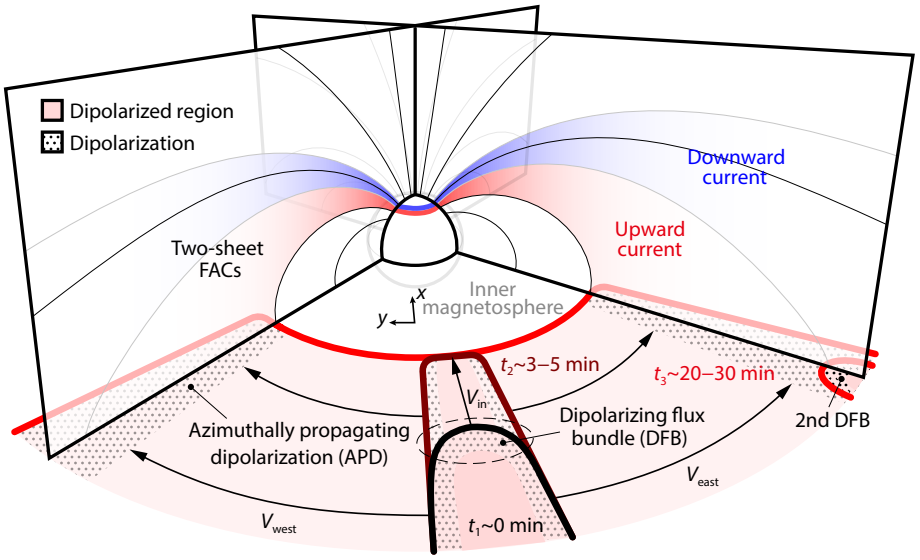

Figure 4. Schematic diagram illustrating the propagation of dipolarization. At t_1 ~ 0 min, a dipolarization is initiated in the magnetotail. The front part of the dipolarized region is the DFB (circled). It propagates earthward, following the BBF and reaching the inner-magnetosphere in t_2 ~3–5 min. Meanwhile, the two sides of the dipolarized region are the azimuthally propagating global-scale dipolarizations (APDs). They propagate eastward and westward, following the global convection and reaching the dayside in t_3 ~20–30 min. Two-sheet FACs are coupled to the global-scale dipolarization. The downward current sheet is at higher latitudes than the upward current sheet. Multiple DFBs/BBFs can occur around the expanding edge of the dipolarized region. The color of the thick boundaries indicates the time history.

coupled is an important question. According to our observations, meso-scale dipolarizations tend to be observed around the expanding edge of a global-scale dipolarization (Figure 4). This is an interesting coincidence that indicates the global- and meso-scale dipolarizations might be physically coupled. The observed coincidence suggests a scenario in which magnetic energy is released from a global to meso-scale in an azimuthal ordering and a sporadic manner. The strength of the global-scale dipolarization, as quantified by the change in the tilt angle, decreases as it expands azimuthally. Its magnetic energy is ported into the earthward propagating meso-scale dipolarizations and the associated Poynting flux sporadically (Figure 3), possibly through the resonant mode coupling (Southwood, 1974) or the mode conversion around density gradients (Allan and Wright, 2000). The conditions and predictions of these mechanisms can be investigated in future studies.

Another possibility is that the observed coincidence of global- and meso-scale dipolarizations is physically trivial. BBFs/DFBs may deviate from midnight as they propagate earthward because of high magnetic pressure (Gabrielse et al., 2019), thereby appearing on the edge of the global-scale dipolarization. The deviation of BBFs should occur at a certain distance and can be quantified if multiple satellites are in a suitable geometry. Alternatively, Merkin et al. (2019) suggested that the global-scale dipolarization may result from the accumulation of meso-scale dipolarizations. However, in our events, meso-scale dipolarizations appear far less frequently than in their simulation and occur around the edge of global-scale dipolarizations (instead of within the edge).

Here, we note the scope of the discussions and observations mentioned in this study. We tended to observe them during geomagnetic storms, when a major global-scale dipolarization expanded azimuthally and meso-scale dipolarizations occurred around the expanding edge of the global-scale dipolarization. This may be one particular pathway through which magnetic energy stored in the tail is released. There are clearly other pathways that involve other coupling between the global- and meso-scale dipolarizations, as suggested from the ground observations (Nishimura et al., 2020). Therefore, our observations do not rule out other possibilities indicated by previous studies (Gabrielse et al., 2019; Merkin et al., 2019) but suggest the diversity and complexity of the energy release pathways. It would be interesting to investigate the different cross-scale couplings and the conditions of their occurrence to gain a deeper understanding of the underlying physics. Our approach of combining multiple satellites to 2D ionospheric currents is shown here to be an efficient means of gathering more information. The Energetic Neutral Atom (ENA) imaging of the plasma sheet (Keesee et al., 2021) may be another promising tool to visualize the evolution of global- and meso-scale dipolarizations.

Recent observations from Juno revealed that Jupiter's dawn storm shared many fundamental features with the auroral signatures of the substorms at Earth (Bonfond et al., 2021), there are cross-scale auroral features that develop similarly to the global- and meso-scale dipolarizations reported here. On Jupiter, large-scale auroral brightening often expands azimuthally to a global scale. Likewise, there are smaller-scale auroral features that develop to lower latitudes, similar to the auroral streamers on Earth, which are associated with BBFs. Despite the substantial differences between the dynamics of the magnetospheres at Earth and Jupiter, these similar features highlight that the cross-scale energy release processes might be universal in planetary plasmas. Our understanding of the different cross-scale couplings on Earth may apply to understanding similar features on other planets.

4. Conclusions

In conclusion, with the new approach of combining a network of magnetospheric satellites and 2D ground observations, we determined the propagation of individual global-scale dipolarizations. As illustrated graphically in Figure 4, the azimuthal propagation is enduring (20–30 min), slow (2–4 deg/min), and global (12 h in MLT). It is likely a result of the global convection, which has a similar flow direction, speed, and spatial extent. At a certain MLT, the global-scale dipolarization maps to an upward FAC, which connects the auroral oval in the ionosphere and the equator over a broad range of distances. The azimuthal and divergent propagation of this magnetosphere–ionosphere coupled system develops into global-scale two-sheet FACs and a westward Hall auroral electrojet. On the other hand, meso-scale dipolarizations and the associated processes (BBF, SCW, Poynting flux bursts) are related to impulsive energy release. According to our observations, these processes tend to emerge around the expanding edges of the global-scale dipolarization (Figure 4).

The events we studied here occurred during geomagnetic storms. The coupling between meso-scale and global-scale dipolarizations reported here is often seen in other storms. It would be useful to investigate the coupling in non-storm times, as other cross-scale coupling mechanisms may also exist (e.g., Gabrielse et al., 2019; Nishimura et al., 2020). Our approach of combining 2D ionospheric currents with a network of magnetospheric satellites provides a new perspective for investigating the potential cross-scale couplings in the magnetosphere–ionosphere system.

Open Research

The data used in this study are available online. The THEMIS spacecraft and all-sky imager data are available at https://cdaweb.gsfc.nasa.gov/pub/data/themis/. The MMS data are available at https://cdaweb.gsfc.nasa.gov/pub/data/mms/. The GOES data are available at https://cdaweb.gsfc.nasa.gov/pub/data/goes. The RBSP data are available athttps://cdaweb.gsfc.nasa.gov/pub/data/rbsp/. The ionospheric current data are available athttps://cdaweb.gsfc.nasa.gov/pub/data/aaa_special-purpose-datasets/spherical-elementary-and-equivalent-ionospheric-currents-weygand.

Acknowledgements

We thank the following spacecraft missions and relevant instrument teams for providing the data used in this study, including the THEMIS all-sky imagers and ground magnetometers, the FGM (Fluxgate Magnetometer), EFI (Electric Field Instrument), and ESA (Electrostatic Analyzer) instruments onboard THEMIS; the magnetometer and particle instrument onboard GOES; the EMFISIS (Electric and Magnetic Field Instrument Suite and Integrated Science), EFW (Electric Field and Waves Suite), HOPE (Helium, Oxygen, Proton and Electron Mass Spectrometer), and MagEIS (Magnetic Electron Ion Spectrometer) instruments onboard RBSP; the FGM instrument onboard MMS; and the particle instrument onboard LANL 1991-080. S. Tian acknowledges NASA (National Aeronautics and Space Administration) grant 81NSSC19K0306 and NASA prime contract NAS5-01072. J. Liu acknowledges AFOSR (Air Force Office of Scientific Research) grant FA9559-16-1-0364; NSF (National Science Foundation) grant AGS-2055192; NASA grants 80NSSC20K1314, 80NSSC20K1316, and 80NSSC21K1407; and NASA Contract NAS5-02099. J. M. Weygand acknowledges NASA grants: 80NSSC18K1220 and 80NSSC18K0570, NASA contracts 80GSFC17C0018, and NAS5-02099. J. Bortnik acknowledges NASA award 80NSSC18K1227. S. Tian sincerely thanks M. K. Hudson, L. R. Lyons, A. Runov, and X. Chu for helpful suggestions related to this study.

Supplementary Materials

Algorithm of the Three-Satellite Timing and Dipolarization Identification

A1 Three-satellite Timing

The three-satellite timing is illustrated in Figure A1. $\boldsymbol{v}_n$, the 2D speed of a phase front of dipolarization in the equatorial plane, can be determined by

$$\begin{aligned}(\boldsymbol{r}_1-\boldsymbol{r}_2)\cdot\hat{v}_n &= |\boldsymbol{v}_n|(t_1-t_2)\\ (\boldsymbol{r}_1-\boldsymbol{r}_3)\cdot\hat{v}_n &= |\boldsymbol{v}_n|(t_1-t_3)\end{aligned}, \tag{A1}$$

where $t_{1,2,3}$ is the time when the phase front is observed at spacecraft 1, 2, and 3 and $\boldsymbol{r}_{1,2,3}$ is the corresponding location. This is a linear equation in $\hat{v}_n/|\boldsymbol{v}_n|$, which is solvable when 1, 2, and 3 are non-collinear. $\boldsymbol{v}_n$ is then obtained from $\hat{v}_n/|\boldsymbol{v}_n|$. Non-collinearity requires that a triangle formed by the 3 spacecraft cannot be too acute or too obtuse. Below we describe how t_i is determined.

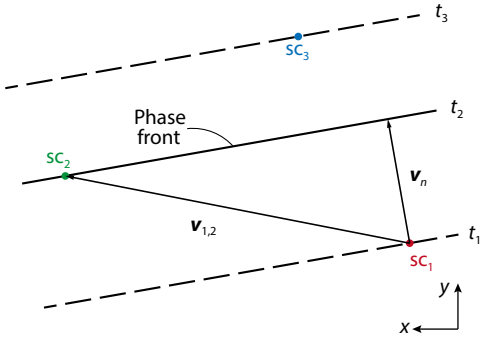

Figure A1. Measuring the 2D propagation speed $\boldsymbol{v}_n$ of a dipolarization in the *x*-*y* plane by using three non-collinear spacecraft (SC). Note that the phase velocity $|\boldsymbol{v}_{1,2}|$ measured by a two-spacecraft timing is generally larger than $|\boldsymbol{v}_n|$, especially when the spacecraft separation is perpendicular to $\boldsymbol{v}_{1,2}$.

A2 Dipolarization Identification

A dipolarization is defined as the sudden increase of α, the tilt angle of the magnetic field, where $\alpha = \arcsin(B_z/|B|)$ and $B_{x,y,z}$ are the magnetic field components in the solar magnetic (SM) coordinate system. To compare dipolarizations at different distances, we need to remove the background of α attributable to the Earth's dipole magnetic field. In this study, we estimate the background by using the T89 model) and a further boxcar average over 60 min (Figure A2). The detrended tilt angle θ is the data we focus on (Figure A2b).

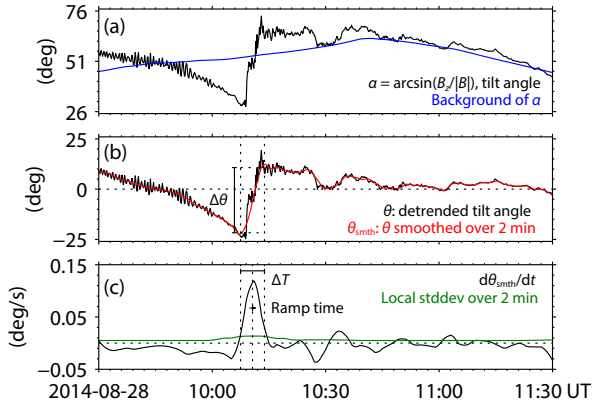

Figure A2. An example showing the algorithm to detect a ramp of increasing tilt angle and determine its properties. Panel (a) shows the tilt angle α calculated from the measured magnetic field in the solar magnetic (SM) coordinate system. The T89 model of the Earth's magnetic field is subtracted, and the result is detrended using a boxcar average over 60 min. Panel (b) shows the detrended tilt angle θ. A dipolarization corresponds to a positive slope centered around 0. To focus on the main ramp associated with a dipolarization, the tilt angle is smoothed over 2 min to remove small-scale fluctuations. Panel (c) shows the derivative of the smoothed θ (black) and its local standard deviation over 2 min (green). The start and end times (t_S and t_E) of the ramp are identified as where $d\theta/dt$ exceeds the local standard deviation by one sigma. Consequently, we define the duration $\Delta T = t_E - t_S$, the change in tilt angle $\Delta\theta = \theta(t_E) - \theta(t_S)$, and the "ramp time" $= (t_E + t_S)/2$ for the ramp.

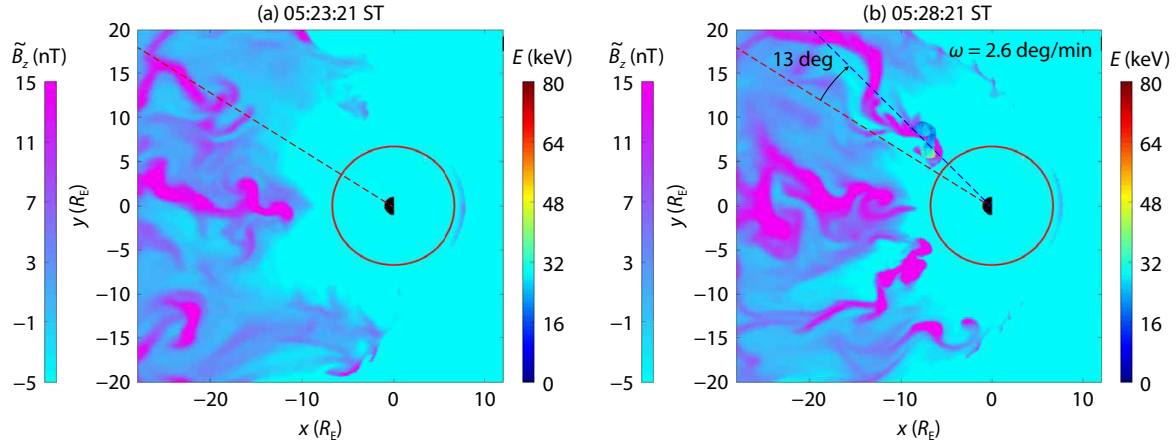

Figure A3. Snapshots from Movie S1 of Eshetu et al. (2019). The dashed lines mark the local times of a dipolarized region at the times shown. During the 5 min, the earthward head of the region (i.e., the DFB), moved earthward from approximately 15 R_E to 5 R_E. In addition, the dipolarized region rotated 13 deg, corresponding to an angular speed of 2.6 deg/min. The cause of the drift is the convection electric field in the simulation.

Dipolarization corresponds to the ramp of increasing θ. To quantify the parameters of the ramp, we define (1) the start and end times (t_S and t_{Ei}), where $d\theta/dt$ exceeds its local standard deviation by 1 sigma (Figure A2c); (2) the duration $\Delta T = t_E - t_S$; (3) the strength $\Delta\theta = \theta(t_E) - \theta(t_S)$; and (4) the "ramp time" $= (t_E + t_S)/2$. To remove small scale fluctuations on top of the main ramp, θ is smoothed over a 2-min window (non-smoothed θ are used in all other calculations). The smoothed version is shown in Figure A2b (red). The ramp times are used as t_i in Equation (1) to solve for the propagation velocity $\boldsymbol{v}_n$. For example, the gray arrow in Figure 1d marks the $\boldsymbol{v}_n$ determined for the gray triangle formed by G15, THD, and THE. The gray arrow starts from the center of the triangle, representing the $\boldsymbol{v}_n$ for the covered space. The propagation speed $\boldsymbol{v}_n$ has been determined in other triangles formed by different spacecraft combinations (e.g., RBB, G15, and THA). They are not shown because they are all azimuthal and with comparable magnitudes to the shown gray vector shown.

References

Allan, W., and Wright, A. N. (2000). Magnetotail waveguide: Fast and Alfvén waves in the plasma sheet boundary layer and lobe. *J. Geophys. Res.: Space Phys.*, *105*(A1), 317–328. https://doi.org/10.1029/1999JA900425

Amm, O., and Viljanen, A. (1999). Ionospheric disturbance magnetic field continuation from the ground to the ionosphere using spherical elementary current systems. *Earth Planets Space*, *51*(6), 431–440. https://doi.org/10.1186/BF03352247

Angelopoulos, V., Baumjohann, W., Kennel, C. F., Coroniti, F. V., Kivelson, M. G., Pellat, R., Walker, R. J., Lühr, H., and Paschmann, G. (1992). Bursty bulk flows in the inner central plasma sheet. *J. Geophys. Res.: Space Phys.*, *97*(A4), 4027–4039. https://doi.org/10.1029/91JA02701

Angelopoulos, V., Sibeck, D., Carlson, C. W., McFadden, J. P., Larson, D., Lin, R. P., Bonnell, J. W., Mozer, F. S., Ergun, R., … Sigwarth, J. (2008). First results from the THEMIS mission. *Space Sci. Rev.*, *141*(1–4), 453–476. https://doi.org/10.1007/s11214-008-9378-4

Auster, H. U., Glassmeier, K. H., Magnes, W., Aydogar, O., Baumjohann, W., Constantinescu, D., Fischer, D., Fornacon, K. H., Georgescu, E., … Wiedemann, M. (2008). The THEMIS fluxgate magnetometer. *Space Sci. Rev.*,

141(1–4), 235–264. https://doi.org/10.1007/s11214-008-9365-9

Baumjohann, W., Paschmann, G., and Lühr, H. (1990). Characteristics of high-speed ion flows in the plasma sheet. *J. Geophys. Res.: Space Phys.*, *95*(A4), 3801–3809. https://doi.org/10.1029/JA095iA04p03801

Baumjohann, W., Hesse, M., Kokubun, S., Mukai, T., Nagai, T., and Petrukovich, A. A. (1999). Substorm dipolarization and recovery. *J. Geophys. Res.: Space Phys.*, *104*(A11), 24995–25000. https://doi.org/10.1029/1999JA900282

Bonfond, B., Yao, Z. H., Gladstone, G. R., Grodent, D., Gérard, J. C., Matar, J., Palmaerts, B., Greathouse, T. K., Hue, V., … Bolton, S. J. (2021). Are dawn storms Jupiter's auroral substorms?. *AGU Adv.*, *2*(1), e2020AV000275. https://doi.org/10.1029/2020AV000275

Boström, R. (1964). A model of the auroral electrojets. *J. Geophys. Res.*, *69*(23), 4983–4999. https://doi.org/10.1029/JZ069i023p04983

Clauer, C. R., and McPherron, R. L. (1974). Mapping the local time-universal time development of magnetospheric substorms using mid-latitude magnetic observations. *J. Geophys. Res.*, *79*(19), 2811–2820. https://doi.org/10.1029/JA079i019p02811

Cummings, W. D., Barfield, J. N., and Coleman, P. J. Jr. (1968). Magnetospheric substorms observed at the synchronous orbit. *J. Geophys. Res.*, *73*(21), 6687–6698. https://doi.org/10.1029/JA073i021p06687

Dungey, J. W. (1961). Interplanetary magnetic field and the auroral zones. *Phys. Rev. Lett.*, *6*(2), 47–48. https://doi.org/10.1103/PhysRevLett.6.47

Eshetu, W. W., Lyon, J. G., Hudson, M. K., and Wiltberger, M. J. (2019). Simulations of electron energization and injection by BBFs using high-resolution LFM MHD fields. *J. Geophys. Res.: Space Phys.*, *124*(2), 1222–1238. https://doi.org/10.1029/2018JA025789

Fujii, R., Hoffman, R. A., Anderson, P. C., Craven, J. D., Sugiura, M., Frank, L. A., and Maynard, N. C. (1994). Electrodynamic parameters in the nighttime sector during auroral substorms. *J. Geophys. Res.: Space Phys.*, *99*(A4), 6093–6112. https://doi.org/10.1029/93JA02210

Gabrielse, C., Angelopoulos, V., Harris, C., Artemyev, A., Kepko, L., and Runov, A. (2017). Extensive electron transport and energization via multiple, localized dipolarizing flux bundles. *J. Geophys. Res.: Space Phys.*, *122*(5), 5059–5076. https://doi.org/10.1002/2017JA023981

Gabrielse, C., Spanswick, E., Artemyev, A., Nishimura, Y., Runov, A., Lyons, L., Angelopoulos, V., Turner, D. L., Reeves, G. D., … Donovan, E. (2019). Utilizing the heliophysics/geospace system observatory to understand particle injections: Their scale sizes and propagation directions. *J. Geophys. Res.: Space Phys.*, *124*(7), 5584–5609. https://doi.org/10.1029/2018JA025588

Iijima, T., and Potemra, T. A. (1978). Large-scale characteristics of field-aligned currents associated with substorms. *J. Geophys. Res.: Space Phys.*, *83*(A2), 599–615. https://doi.org/10.1029/JA083iA02p00599

Keesee, A. M., Buzulukova, N., Mouikis, C., and Scime, E. E. (2021). Mesoscale structures in Earth's magnetotail observed using energetic neutral atom imaging. *Geophys. Res. Lett.*, *48*(3), e2020GL091467. https://doi.org/10.1029/2020GL091467

Keiling, A., Wygant, J. R., Cattell, C. A., Mozer, F. S., and Russell, C. T. (2003). The global morphology of wave Poynting flux: Powering the aurora. *Science*, *299*(5605), 383–386. https://doi.org/10.1126/science.1080073

Kepko, L., McPherron, R. L., Amm, O., Apatenkov, S., Baumjohann, W., Birn, J., Lester, M., Nakamura, R., Pulkkinen, T. I., and Sergeev, V. (2015). Substorm current wedge revisited. *Space Sci. Rev.*, *190*(1–4), 1–46. https://doi.org/10.1007/s11214-014-0124-9

Kissinger, J., McPherron, R. L., Hsu, T. S., and Angelopoulos, V. (2012). Diversion of plasma due to high pressure in the inner magnetosphere during steady magnetospheric convection. *J. Geophys. Res.: Space Phys.*, *117*(A5), A05206. https://doi.org/10.1029/2012JA017579

Kletzing, C. A., Kurth, W. S., Acuna, M., MacDowall, R. J., Torbert, R. B., Averkamp, T., Bodet, D., Bounds, S. R., Chutter, M., … Tyler, J. (2013). The electric and magnetic field instrument suite and integrated science (EMFISIS) on RBSP. *Space Sci. Rev.*, *179*(1–4), 127–181. https://doi.org/10.1007/s11214-013-9993-6

Liu, J., Angelopoulos, V., Runov, A., and Zhou, X. Z. (2013). On the current sheets surrounding dipolarizing flux bundles in the magnetotail: The case for wedgelets. *J. Geophys. Res.: Space Phys.*, *118*(5), 2000–2020. https://doi.org/10.1002/jgra.50092

Liu, J., Angelopoulos, V., Zhou, X. Z., and Runov, A. (2014). Magnetic flux transport by dipolarizing flux bundles. *J. Geophys. Res.: Space Phys.*, *119*(2), 909–926. https://doi.org/10.1002/2013JA019395

Liu, J., Angelopoulos, V., Chu, X. N., Zhou, X. Z., and Yue, C. (2015). Substorm current wedge composition by wedgelets. *Geophys. Res. Lett.*, *42*(6), 1669–1676. https://doi.org/10.1002/2015GL063289

McPherron, R. L., Russell, C. T., and Aubry, M. P. (1973). Satellite studies of magnetospheric substorms on August 15, 1968: 9. Phenomenological model for substorms. *J. Geophys. Res.*, *78*(16), 3131–3149. https://doi.org/10.1029/JA078i016p03131

Mende, S. B., Harris, S. E., Frey, H. U., Angelopoulos, V., Russell, C. T., Donovan, E., Jackel, B., Greffen, M., and Peticolas, L. M. (2008). The THEMIS array of ground-based observatories for the study of auroral substorms. *Space Sci. Rev.*, *141*(1–4), 357–387. https://doi.org/10.1007/s11214-008-9380-x

Merkin, V. G., Panov, E. V., Sorathia, K. A., and Ukhorskiy, A. Y. (2019). Contribution of bursty bulk flows to the global dipolarization of the magnetotail during an isolated substorm. *J. Geophys. Res.: Space Phys.*, *124*(11), 8647–8668. https://doi.org/10.1029/2019JA026872

Nagai, T. (1982). Observed magnetic substorm signatures at synchronous altitude. *J. Geophys. Res.: Space Phys.*, *87*(A6), 4405–4417. https://doi.org/10.1029/JA087iA06p04405

Nakamura, R., Baumjohann, W., Panov, E., Petrukovich, A. A., Angelopoulos, V., Volwerk, M., Magnes, W., Nishimura, Y., Runov, A., … McFadden, J. (2011). Flux transport, dipolarization, and current sheet evolution during a double-onset substorm. *J. Geophys. Res.: Space Phys.*, *116*(A5), A00I36. https://doi.org/10.1029/2010JA015865

Nishimura, Y., Lyons, L. R., Angelopoulos, V., Kikuchi, T., Zou, S., and Mende, S. B. (2011). Relations between multiple auroral streamers, pre-onset thin arc formation, and substorm auroral onset. *J. Geophys. Res.: Space Phys.*, *116*(A9), A09214. https://doi.org/10.1029/2011JA016768

Nishimura, Y., Lyons, L. R., Gabrielse, C., Weygand, J. M., Donovan, E. F., and Angelopoulos, V. (2020). Relative contributions of large-scale and wedgelet currents in the substorm current wedge. *Earth Planets Space*, *72*, 106. https://doi.org/10.1186/S40623-020-01234-X

Nishimura, Y., Verkhoglyadova, O., Deng, Y., and Zhang, S. R. (2022). *Cross-Scale Coupling and Energy Transfer in the Magnetosphere-Ionosphere-Thermosphere System*. San Diego: Elsevier. https://doi.org/10.1016/C2019-0-00526-2

Ogasawara, K., Kasaba, Y., Nishimura, Y., Hori, T., Takada, T., Miyashita, Y., Angelopoulos, V., Mende, S. B., and Bonnell, J. (2011). Azimuthal auroral expansion associated with fast flows in the near-Earth plasma sheet: Coordinated observations of the THEMIS all-sky imagers and multiple spacecraft. *J. Geophys. Res.: Space Phys.*, *116*(A6), A06209. https://doi.org/10.1029/2010JA016032

Ohtani, S., Motoba, T., Gkioulidou, M., Takahashi, K., and Singer, H. J. (2018). Spatial development of the dipolarization region in the inner magnetosphere. *J. Geophys. Res.: Space Phys.*, *123*(7), 5452–5463. https://doi.org/10.1029/2018JA025443

Runov, A., Angelopoulos, V., Sitnov, M. I., Sergeev, V. A., Bonnell, J., McFadden, J. P., Larson, D., Glassmeier, K. H., and Auster, U. (2009). THEMIS observations of an earthward-propagating dipolarization front. *Geophys. Res. Lett.*, *36*(14), L14106. https://doi.org/10.1029/2009GL038980

Runov, A., Angelopoulos, V., Zhou, X. Z., Zhang, X. J., Li, S., Plaschke, F., and Bonnell, J. (2011). A THEMIS multicase study of dipolarization fronts in the magnetotail plasma sheet. *J. Geophys. Res.: Space Phys.*, *116*(A5), A05216. https://doi.org/10.1029/2010JA016316

Singer, H., Matheson, L., Grubb, R., Newman, A., and Bouwer, D. (1996). Monitoring space weather with the GOES magnetometers. In *Proceedings Volume 2812, Goes-8 and Beyond* (pp. 299–308). Denver, CO, United States: SPIE. https://doi.org/10.1117/12.254077

Southwood, D. J. (1974). Some features of field line resonances in the magnetosphere. *Planet. Space Sci.*, *22*(3), 483–491. https://doi.org/10.1016/0032-0633(74)90078-6

Tian, S., Colpitts, C. A., Wygant, J. R., Cattell, C. A., Ferradas, C. P., Igl, A. B., Larsen,

B. A., Reeves, G. D., and Donovan, E. F. (2021). Evidence of Alfvénic Poynting flux as the primary driver of auroral motion during a geomagnetic substorm. *J. Geophys. Res.: Space Phys.*, *126*(5), e2020JA029019. https://doi.org/10.1029/2020JA029019

Tian, S., Wang, C. P., Lyons, L. R., Bortnik, J., Weygand, J. M., Liu, J., Yadav, S., Ma, Q., Reeves, G. D., … Wolf, R. A. (2023). Multiple auroral streamer bundles in conjugate hemispheres and multiple near-Earth injections. *J. Geophys. Res.: Space Phys.*, *128*(1), e2022JA031010. https://doi.org/10.1029/2022JA031010

Torbert, R. B., Russell, C. T., Magnes, W., Ergun, R. E., Lindqvist, P. A., LeContel, O., Vaith, H., Macri, J., Myers, S., … Lappalainen, K. (2016). The FIELDS instrument suite on MMS: Scientific objectives, measurements, and data products. *Space Sci. Rev.*, *199*(1−4), 105−135. https://doi.org/10.1007/s11214-014-0109-8

Tsyganenko, N. A. (2002). A model of the near magnetosphere with a dawn-dusk asymmetry 1. Mathematical structure. *J. Geophys. Res.: Space Phys.*, *107*(A8), SMP 12-1-SMP 12−5. https://doi.org/10.1029/2001JA000219

Ukhorskiy, A. Y., Sorathia, K. A., Merkin, V. G., Sitnov, M. I., Mitchell, D. G., and Gkioulidou, M. (2018). Ion trapping and acceleration at dipolarization fronts: High-resolution MHD and test-particle simulations. *J. Geophys. Res.: Space Phys.*, *123*(7), 5580−5589. https://doi.org/10.1029/2018JA025370

Vanhamäki, H., and Juusola, L. (2020). Introduction to spherical elementary current systems. In M. W. Dunlop, et al. (Eds.), *Ionospheric Multi-Spacecraft Analysis Tools: Approaches for Deriving Ionospheric Parameters* (pp. 5−33). Cham: Springer. https://doi.org/10.1007/978-3-030-26732-2_2

Wang, C.-P., Lyons, L. R., Weygand, J. M., Nagai, T., and McEntire, R. W. (2006). Equatorial distributions of the plasma sheet ions, their electric and magnetic drifts, and magnetic fields under different interplanetary magnetic field B_z conditions. *J. Geophys. Res.: Space Phys.*, *111*(A4), A04215. https://doi.org/10.1029/2005JA011545

Weygand, J. M., Amm, O., Viljanen, A., Angelopoulos, V., Murr, D., Engebretson, M. J., Gleisner, H., and Mann, I. (2011). Application and validation of the spherical elementary currents systems technique for deriving ionospheric equivalent currents with the North American and Greenland ground magnetometer arrays. *J. Geophys. Res.: Space Phys.*, *116*(A3), A03305. https://doi.org/10.1029/2010JA016177

Wygant, J. R., Keiling, A., Cattell, C. A., Johnson, M., Lysak, R. L., Temerin, M., Mozer, F. S., Kletzing, C. A., Scudder, J. D., … Spann, J. (2000). Polar spacecraft based comparisons of intense electric fields and Poynting flux near and within the plasma sheet-tail lobe boundary to UVI images: An energy source for the aurora. *J. Geophys. Res.*, *105*(A8), 18675−18692. https://doi.org/10.1029/1999JA900500

Yao, Z. H., Sun, W. J., Fu, S. Y., Pu, Z. Y., Liu, J., Angelopoulos, V., Zhang, X. J., Chu, X. N., Shi, Q. Q., … Zong, Q. G. (2013). Current structures associated with dipolarization fronts. *J. Geophys. Res.: Space Phys.*, *118*(11), 6980−6985. https://doi.org/10.1002/2013JA019290